



Dynamic Responses and Failure Behaviors of Saturated Rocks Subjected to Repetitive Compression–Shear Impacting

Hongbo Du^{1,2} · Feng Dai² · Ang Li² · Ruochen Jiang³

Received: 5 April 2022 / Accepted: 6 March 2023 / Published online: 23 March 2023
© The Author(s), under exclusive licence to Springer-Verlag GmbH Austria, part of Springer Nature 2023

Abstract

In waterway regulation engineering, submerged reefs are quite susceptible to the repetitive oblique strike from drop hammer and impact drilling, leading to a repetitive compression–shear impacting. Understanding the dynamic responses and failure mechanism of saturated rocks subjected to repetitive compression–shear impacting is thus of great significance for the efficient removal of submerged reefs. In this study, using the split Hopkinson pressure bar (SHPB) apparatus, the repetitive compression–shear impacting tests were conducted on the saturated and dry sandstone specimen from the harbor excavation project in Guoyuan Port (Chongqing, China). Our experimental results indicate that the increasing loading rate or shear component in the dynamic loading has a negative influence on the bearing capacity of saturated sandstone subjected to repetitive impacting. The deformability of saturated rocks increases as the impacting number or the shear component in the dynamic loading. The energy absorption ability as well as the energy utilization of the saturated rocks is highly improved by implementing repetitive compression–shear impacting, and such improvement yields an ascension limit with the increasing shear component in the dynamic loading. As the shear component introduces into the repetitive impacting loading, the failure patterns of rocks change from the relative tensile mode with a large deformation band along the loading direction to the combined compression–shear mode with two parallel large deformation bands inclined to the loading direction, the water content between the mineral grains promotes the shear failure in rock dynamic testing. These results can provide a better understanding of the dynamic responses and failure properties of saturated rocks subjected to repetitive compression–shear impacting.

Highlights

- Illustrated influences of repetitive compression–shear impacting on the bearing capacity and deformability of saturated and dry rocks.
- Investigated energy dissipation of saturated and dry rocks under repetitive combined compression–shear impacting.
- Revealed failure patterns of saturated and dry rocks under repetitive combined compression–shear impacting.

Keywords Repetitive impacting · Combined compression–shear · Dynamic responses · SHPB · Saturated rocks

✉ Feng Dai
fengdai@scu.edu.cn

¹ National Inland Waterway Regulation Engineering Technology Research Center, Chongqing Jiaotong University, Chongqing 400074, People's Republic of China

² State Key Laboratory of Hydraulics and Mountain River Engineering, Sichuan University, Chengdu 610065, Sichuan, China

³ Department of Civil and Environmental Engineering, The Hong Kong University of Science and Technology, Hong Kong, China

1 Introduction

Inland waterways are developing rapidly to meet the increasing demand for waterway transportation (Bu and Nachtmann 2021) due to their natural advantage, including the large transport capacity (Gharehgozli and Zaerpour 2018), low transportation cost (Fazi et al. 2015), less land occupation, low energy consumption (Bomba and Harrison 2002) and environmentally friendly (Zweers et al. 2019). However, many waterways have an urgent need for improving their

navigation capacity and conditions to ensure the safety of enlarging ships, and then millions of submerged reefs are planned to be removed to broaden and deepen such waterways. Considering the environmental protection, the mechanical methods to break rocks are generally employed in the waterway regulation projects, such as the drop hammer and impact drilling (Ali and Mohammed 2021), in which the submerged reefs are commonly subjected to repetitive impacting. Moreover, the oblique strike of impacting loading and the unpredictable structural surfaces in the rock masses result in a complicated compression–shear loading path (Xu and Dai 2018; Du et al. 2020; Wang et al. 2019 and Dai et al. 2022). Thus, understanding the dynamic responses and failure behaviors of saturated rocks subjected to repetitive compression–shear impacting is of great significance to provide theoretical support for the mechanical removal of submerged reefs.

Submerged reefs are in saturated state, and the moisture content significantly affects the strength and deformation characteristics of rocks. Investigations on the mechanical responses and failure behavior of saturated rocks are receiving increasing attention from scholars. Many efforts have been made to reveal the strength and deformation characteristics of saturated rocks by conducting the quasi-static uniaxial compressive tests (Broch 1979; Baud et al. 2000; Talesnick and Shehadeh 2007; Erguler and Ulusay 2009; Yilmaz 2010). Hawkins and McConnell (1992) first found that the difference between the uniaxial compressive strength of dry and saturated sandstone is 78%, and moisture content sensitivities are dominant influenced by the proportion of quartz and clay minerals in such clay-rich Cretaceous Greensand. The Brazilian tensile strength of limestone in case of dry and water-saturated conditions has been furtherly investigated by Vásárhelyi (2005) and Vásárhelyi and Ván (2006), and similar result has been observed. Moreover, the deformability of water-bearing rocks has been fully studied by conducting numerous experimental tests (Li et al. 2012; Wong et al. 2016; Zhou et al. 2016a, 2016b, 2017). They found that its peak cohesion increased by about 14% and the friction angle decreased by 10% as the moisture state of the specimen changed from dry to wet. From the above, as the moisture content in the rocks increases, the reduction of strength is found to be induced by the decreasing friction angle, while the increase of deformability is bound up with both the reduction of Young's modulus and increase of Poisson's ratio.

For the mechanical rock breaking in the waterway regulation projects, the submerged reefs are likely subjected to repetitive impacting from the drop hammer and impact drilling. Some researchers have paid attention to the mechanical behavior of rocks under repetitive impact loading. Li et al. (2005) conducted repeated impact tests on granite employing a split Hopkinson pressure bar (SHPB) system;

they reported that the peak stress of the dynamic loads with a fixed duration has a significant influence on the damage of granite. For the energy dissipation, Li et al. (2018a, b) further found that the cumulative energy per unit volume (energy density) of rocks exhibited obvious three-stage evolution during the repeated impact loading tests. For the constitutive models of rocks under repetitive impacting, Tong et al. (2019) observed evident nonlinear dynamic responses and significant plastic deformation of rock specimen, and they accurately characterized the stress–strain curves of rocks under repetitive impacting using a nonlinear granular model (Johnson and Jia 2005). Moreover, the impact fatigue behaviors of laterally confined rocks have been investigated by Wu et al. (2014) and Luo et al. (2016), and the dynamic statistical damage constitutive model based on Weibull distribution has been developed by Wang et al. (2021). However, the dynamic disturbance in such investigations is pure compressive loading rather than the commonly encountered compression–shear impacting in the engineering projects.

The dynamic compression–shear responses of rocks have been revealed by some scholars using a specific SHPB apparatus, which has been modified in two ways: (I) employing an incident bar with a wedge-shaped end as well as two symmetrically distributed transmitted bars (Zhao et al. 2012), and (II) adding two cushions with designed beveled surfaces between the bar-specimen interfaces (Hou et al. 2011, 2019; Zhao et al. 2011; Xu et al. 2015). They found that the bearing capacity, deformation properties, and fracture patterns of rocks are highly dependent on the shear component in the dynamic loading. Such methods are complicated and costly. Recently, Xu and Dai (2018) provided a more convenient way, the inclined specimens, to realize the compression–shear impacting in rock dynamic testing, and later introduced it into the coupled static–dynamic tests (Xu et al. 2020, 2021) and triaxial dynamic tests (Du et al. 2020, 2021) to reveal the combined dynamic compression–shear responses and failure properties of rocks in the underground engineering. They found that the shear component in the dynamic loading reduces the bearing capacity of statically pressurized rocks, and the failure mechanism is quite different from that subjected to pure dynamic compressive loading.

In the mechanical rock breaking in the waterway regulation projects, the submerged reefs are in saturated state and commonly subjected to repetitive oblique impacting. Thus, the dynamic response and failure behavior of saturated rocks under repetitive compression–shear impacting has an urgent need to be investigated. In this study, using the SHPB apparatus, the repetitive impacting tests are conducted on the saturated sandstone specimen (from the harbor excavation project in Guoyuan Port, Chongqing, China) with different tilting angles of 0°, 3°, 5°, and 7° at the loading rates of 700, 950, and 1200GPa/s. The dynamic mechanical responses

and failure mechanism of saturated sandstone under repetitive combined compression–shear impacting are systematically analyzed, including bearing capacity, deformation properties, energy dissipation, and failure patterns. Section 2 presents the testing apparatus, data processing methods, and preparation of rock specimens. Section 3 presents the experimental results, including dynamic stress equilibrium, strength and deformation characteristics, energy dissipation, and failure patterns. Section 4 concludes this study.

2 Methods and Materials

2.1 Testing Apparatus

The split Hopkinson pressure bar system is a standard and widely used testing apparatus for characterizing the mechanical behavior of materials under high loading rates (Zhou et al. 2012; Du et al. 2018; Xiao et al. 2019; Feng et al. 2021). In this study, the SHPB was utilized to apply the dynamic loading, and its schematic diagram and photograph are shown in Fig. 1. This apparatus mainly consists of striker, incident, and transmitted bar, whose diameter is 50 mm and lengths are 0.3 m, 3 m, and 2 m, respectively. These three bars are made of ultra-high strength steel, whose density (ρ) and Young's modulus (E_b) are 7800 kg/m³ and 221 GPa, respectively. With the help of the locating device, the specimen coated with lubricant at

both ends was installed between the incident and transmitted bars before each impact. Furthermore, a piece copper disk 15 mm in diameter and 3 mm in thickness was mounted on the free end of the incident bar serving as the pulse shaper, which mitigated the rising front and eliminated the high-frequency oscillation of the incident stress wave to facilitate the dynamic stress equilibrium in the specimen (Frew et al. 2002). The compressed air stored in the pressure tank was released to launch the strike, which imposed on the shaper to generate a ramped compressive wave (ϵ_i) propagating in the incident bar. When the stress wave arrives at the interface between the bars and specimen, part of it is reflected into the incident bar forming the reflected wave (ϵ_r), and the transmission part forms transmitted wave (ϵ_t) propagating in the transmitted bar. In addition, the three stress waves were monitored by the strain gauges adhered to the middle position of bars, and the forces applied on the two ends of the specimen can be deduced from the strain signals according to an appropriate wave theory (Kolsky 1949). The force on the incident end of the specimen (P_1) can be derived from the superposition of incident and reflected stress waves, and the force on the transmitted end of the specimen (P_2) can be represented by the transmitted wave.

$$P_1 = A_b E_b (\epsilon_i + \epsilon_r); P_2 = A_b E_b \epsilon_t, \quad (1)$$

where A_b is the cross-sectional area of bars. Once the dynamic force balance was satisfied ($P_1 = P_2$), the dynamic

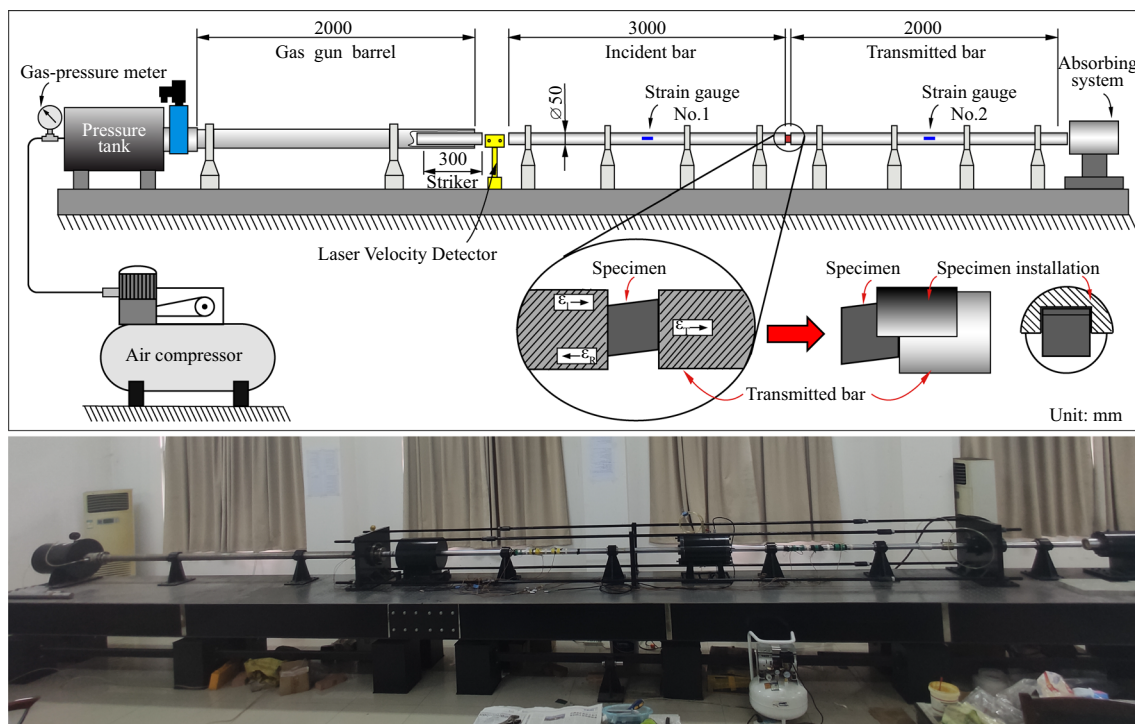


Fig. 1 The schematic diagram and photograph of split Hopkinson pressure bar (SHPB)

stress and strain of the specimen can be calculated (Zhou et al. 2012).

$$\begin{cases} \sigma(t) = \frac{A_b}{2A_0} E_b (\varepsilon_i + \varepsilon_r + \varepsilon_t) \\ \varepsilon(t) = \frac{C}{L} \int_0^t (\varepsilon_i - \varepsilon_t - \varepsilon_r) dt \end{cases}, \quad (2)$$

where C is the P-wave velocity of the steel bar, and L is the length of the specimen, and A_0 denotes the contact area between specimen and bar.

In the conventional SHPB tests, the incident (W_i), reflected (W_r) and transmitted (W_t) energies can be deduced by the following formula (Hong et al. 2009; You et al. 2022 and Li et al. 2019):

$$\begin{cases} W_i = \frac{A_b E_b^2}{\rho C} \int_0^t \varepsilon_i^2 dt \\ W_t = \frac{A_b E_b^2}{\rho C} \int_0^t \varepsilon_t^2 dt \\ W_r = \frac{A_b E_b^2}{\rho C} \int_0^t \varepsilon_r^2 dt \end{cases}. \quad (3)$$

According to the first law of thermodynamics, the total energy absorbed by the specimen (W_a) can be calculated:

$$W_a = W_i - W_t - W_r. \quad (4)$$

This absorbed energy was mainly utilized for the initiation, coalescence, and propagation of cracks, and a minor part was dissipated in other forms, such as thermal energy and radiation energy, which can be ignored in the experiment. Due to the machining tolerance and size difference of these specimens, the dissipation energy per unit volume (i.e., the energy density, W_v) and the energy utilization (η) were employed to reveal the relative magnitude of dissipation energy:

$$W_v = \frac{W_a}{V}; \eta = \frac{W_a}{W_i}. \quad (5)$$

2.2 Specimens and Materials

In this study, the tested specimen is saturated sandstone extracted from the Harbor Excavation Project in Guoyuan Port located in Chongqing, China (shown in Fig. 2). According to the suggested method for the rock dynamic compression test developed by the International Society for Rock Mechanics (ISRM), the rock mass was sliced into cuboid specimens with the same side length of 30 mm, while the heights of specimens are 31, 32, 33 and 34 mm, respectively. Then, both ends of these specimens were polished

to form different tilting angles of 0°, 3°, 5°, and 7° (i.e., the angle between the axial of the specimen and the dynamic loading direction). Moreover, the flatness and parallelism deviations of the specimen ends are limited to 0.05 mm and 0.1°, respectively. A total of 24 specimens were prepared for the repetitive compression–shear impacting tests. The static compression tests are conducted on 0°, 3°, 5°, and 7° specimens using the MTS-810 system in Chongqing Jiaotong University, and the stress–strain curves are illustrated in Fig. 3. Table 1 lists the essential physical and mechanical parameters of saturated sandstone under static coupled compression–shear loading.

In addition, an optical full-field strain mapping technique, the digital image correlation (DIC), has been employed to reveal the failure process of saturated rocks subjected to repetitive compression–shear impact loading. For a high calculation accuracy, the surface of the specimen (i.e., the region of interest) was first painted with a white base coat and subsequently sprayed a contrasting random speckle pattern. The photograph of the painted surface after each impact was captured using the high-speed camera, and the movement of speckles and the full-field strain of this surface can be calculated using an open-source DIC algorithm (Yan et al. 2020). Subsequently, the failure process and failure patterns of saturated rock under repetitive compression–shear impacting can be illustrated.

3 Results and Discussion

3.1 Dynamic Stress Equilibrium

Before the data processing, the fundamental assumption of the rock dynamic test should be verified, i.e., the dynamic stress balance of the specimen. Figure 4 demonstrated the dynamic stress evolution of the 0° specimen under the loading rate of ~950 GPa/s at different impact numbers, where I , R , and T stand for the incident, reflected, and transmitted stress wave, respectively. The superposition of incident and reflected stress waves was represented by $I+R$. The stress in the incident end of the specimen is consistent with that on the transmitted end during the dynamic loading stage. For a better evaluation on the dynamic stress equilibrium, the dynamic stress equilibrium coefficient (i.e., $\mu = \frac{2(P_1 - P_2)}{P_1 + P_2}$) has been introduced in this study, and the time variation of μ was demonstrated using the dotted line. After a fluctuation at the initial stage, the equilibrium coefficient undulates around zero with the amplitudes smaller than the fluctuation threshold, indicating that the dynamic stress equilibrium of 0° specimen under repetitive impacting was achieved. Similar evolution for 7° specimen under the loading rate of ~700 GPa/s can be observed in Fig. 5. These results suggest that

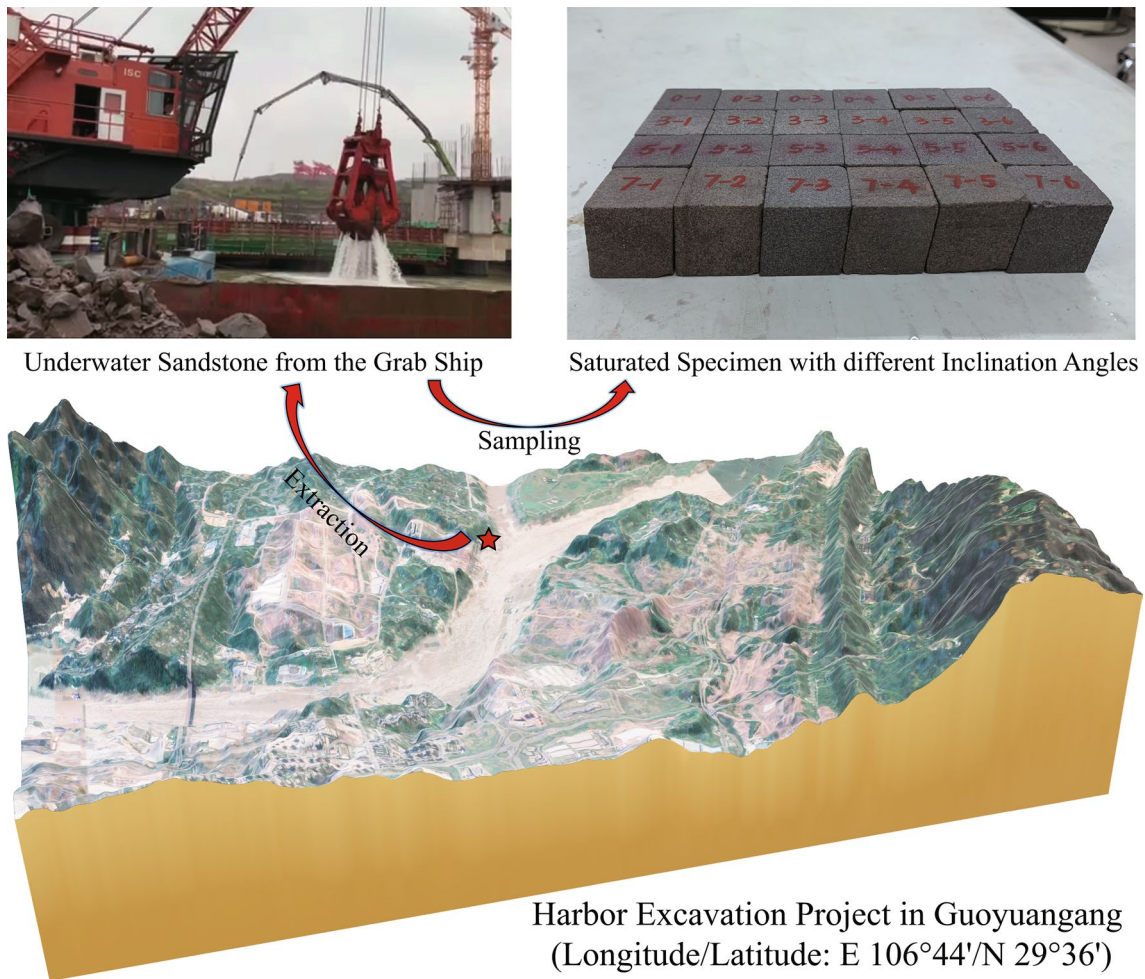


Fig. 2 Harbor Excavation Project in Guoyuan Port (Chongqing, China) and the prepared sandstone specimens

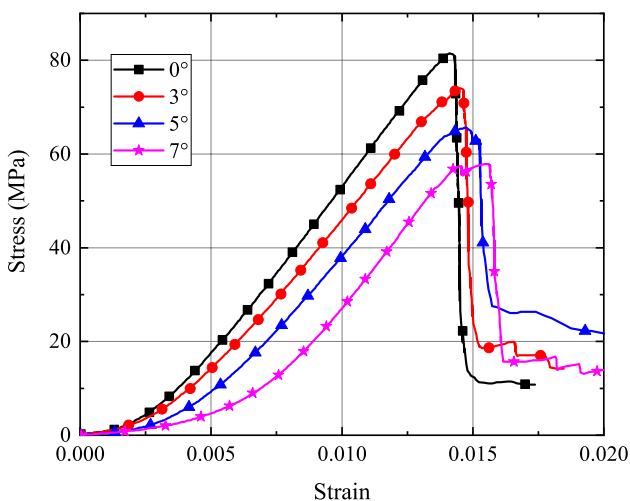


Fig. 3 The stress–strain curves of saturated sandstone specimen under static coupled compression–shear loading

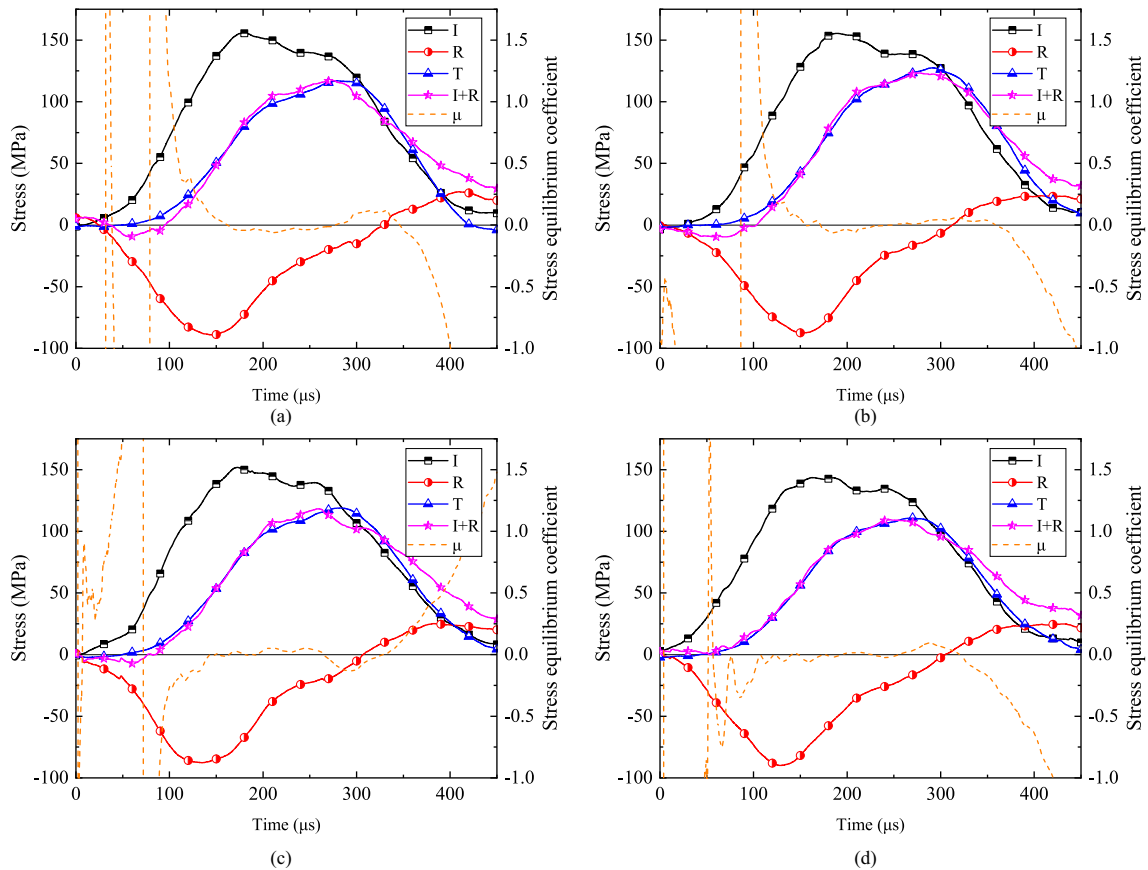
the dynamic stress equilibrium of the saturated rock specimen subjected to repetitive compression–shear impacting can be finely satisfied and the data processing method in Sect. 2.1 can be used in this study.

3.2 Strength and Deformation Characteristics

Figures 6, 7 and 8 exhibit the dynamic stress–strain curves of saturated sandstone specimens with different tilting angles subjected to repetitive impacting at the loading rates of 700, 950, and 1200 GPa/s, respectively. Initially, stress–strain curves for the same tilting angle but different impact numbers experience a short concave upward increasing, which is followed by linear increasing parts with different slopes. Note that the slopes of linear parts increase for the first several impacts and then decrease with the continuously impact, especially for the final several impacts. Subsequently, the stress–strain curves experience a short nonlinear increasing period to the peak values (i.e., peak stress), which is commonly employed to represent the bearing capacity of

Table 1 Some static essential physical and mechanical parameters of saturated sandstone under coupled compression–shear loading

Tilting angle (°)	Density (kg/m ³)	Water content	Peak stress (MPa)	Peak strain (%)	Deformation modulus (GPa)
0	2381	4.38%	81.50	1.41	7.24
3			73.99	1.45	6.54
5			65.65	1.47	6.25
7			57.88	1.56	5.58

**Fig. 4** Dynamic stress equilibrium of 0° specimen under the loading rate of -950 GPa/s at **a** 1st impact, **b** 4th impact, **c** 7th impact and **d** 11th impact

the rock specimen, and the corresponding dynamic strain is likely defined as peak strain. For the unloading stage, the stress first decreased with an increasing strain and finished by a decreasing with a decreasing strain due to the rebound effect. As the repetitive impacting, the rebound effect became more inconspicuous, and the specimen lost its bearing capacity after several impacts.

Figure 9 shows the total impact number of saturated and dry 0°, 3°, 5°, and 7° specimen under different loading rates. For the specimen with different tilting angles, the repetitive impact number decrease significantly as the loading rate increases from 700 to 1200 GPa/s, indicating that the increasing loading rate has a negative influence on the

endurance of saturated sandstone subjected to the repetitive compression–shear impacting. Furthermore, the inclination angle of the specimen is inversely proportional to the total impact number, and this phenomenon suggests that the bearing capacity of sandstone under impacting loading decreases with the increasing shear composition in the dynamic loading. The bearing capacity of sandstone reduces as the water content in the specimen changed from dry condition to saturated condition, and the decrement decreases for a higher loading rate or larger tilting angle. It can thus be concluded that the weakened effect of water content on the endurance of sandstone is severely suppressed by the increasing shear

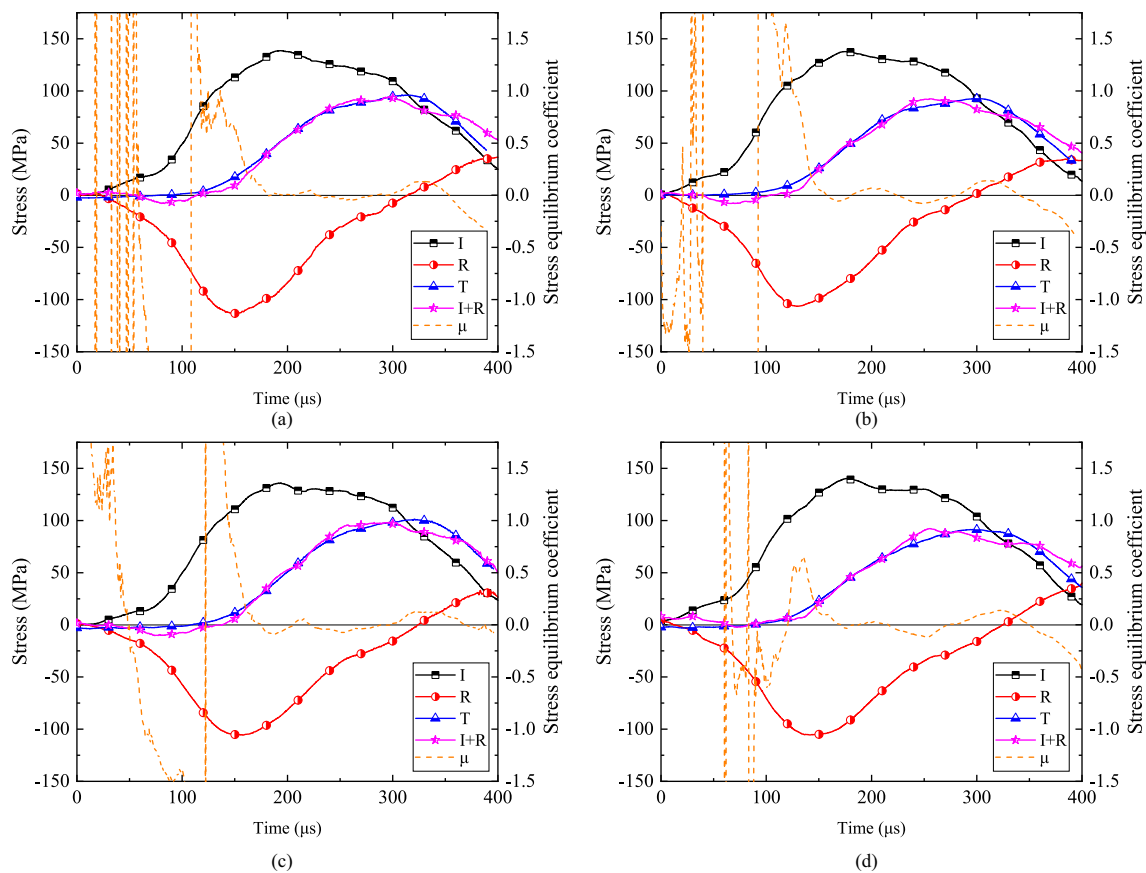


Fig. 5 Dynamic stress equilibrium of 7° specimen under the loading rate of ~700 GPa/s at **a** 1st impact, **b** 3rd impact, **c** 6th impact and **d** 9th impact

composition in dynamic loading and the increasing loading rate.

Figures 10 and 11 plot the dynamic peak stress and peak strain of saturated and dry inclined specimens under repetitive impacting at the loading rate of ~700, ~950, and ~1200 GPa/s, respectively. The peak stresses are almost 1.5 times larger than these in static tests (Table 1). The dynamic peak stresses of dry specimen under repetitive impacting are much larger than those of saturated specimen, and such disparity decreases as the shear composition in dynamic loading increases. As the impact number increases, the peak stress of rock first increases slightly, then almost remains constant, and decreases rapidly in the final several impacts. It implies that both saturated and dry rocks were first compacted by the repetitive impacting loading, and then experienced a stable damage process, followed by an accelerated damage process. For a given loading rate, the strength envelope shrinks inward as the tilting angle of the specimen increases, suggesting that the dynamic peak stress decreases with the increasing tilting angle of the specimen, and the decrement is more obvious in the lower loading rate condition. This indicates that the bearing capacity of saturated rocks

is reduced by the shear component in the dynamic repetitive impacting. Thus, the dynamic shear loading should be introduced in the repetitive impacting for a better mechanical rock breaking in the waterway regulation, and the oblique strike of the drop hammer and impact drilling might be an effective means for the realization of repetitive compression–shear impacting.

As shown in Fig. 11, the peak strain of saturated and dry inclined specimens under repetitive impacting slightly decreases at the first several impacts due to the compaction effect, and then the peak strain increases stably to the failure stage. For an approximate loading rate, the peak strain increases as the tilting angle of the specimen increases. Figure 12 demonstrated the dynamic deformation modulus of saturated and dry rocks (determined from the linear port of the dynamic stress–strain curves of 0° specimens) under repetitive impacting at the different loading rates, which are almost three times larger than these in static tests (Table 1) possibly due to the inertial effect. Similarly, the dynamic Young’s modulus increases at the first several impacts due to the compaction effect, and then experienced a slight decrease stage to the rapid decrease stage, indicating that

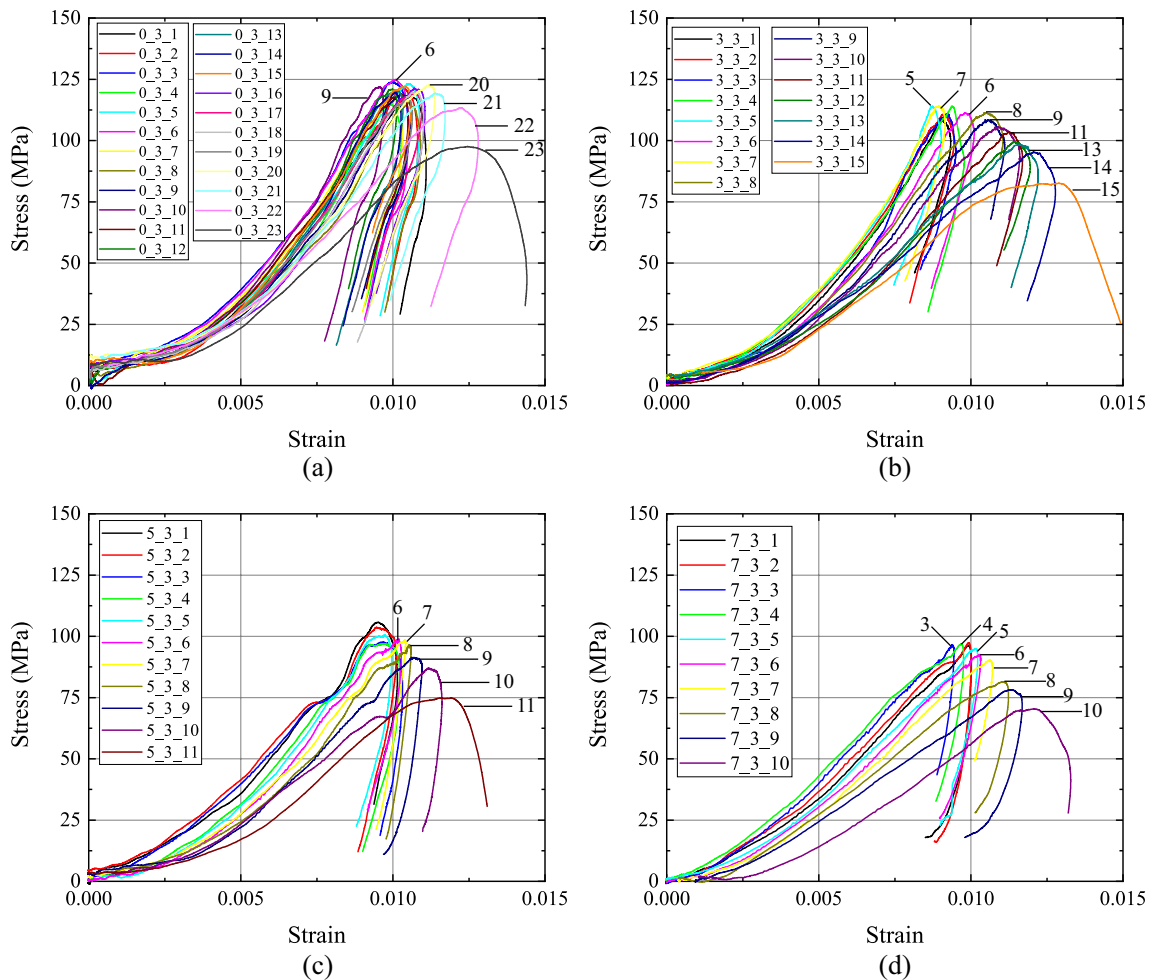


Fig. 6 Stress–strain curves of **a** 0°, **b** 3°, **c** 5° and **d** 7° specimen under the dynamic loading rate of ~700 GPa/s

the specimen suffered irreversible damage due to the repetitive impacts. The dry samples yield a higher modulus than the saturated ones, and the water content in the specimen has a softening effect on rocks. The modulus seems to be constant under different loading rates for both saturated and dry conditions, and it means that the Young's modulus of sandstone subjected to repetitive compression–shear impacting is not sensitive to loading rates.

Sandstone consists of mineral grains and cement between grains. For saturated rocks, several physical and chemical reactions (Cai et al. 2020; Wasantha et al. 2018) would take place inner the minerals and cement, resulting the increasingly loose of rock structures and the gradually weakening of grains cementation. Besides, the free water decreases the friction between the grains (Cai et al. 2019; Kawai et al. 2015), and further promotes the slide of cracks. The above two points make a large contribution to the reduction of the strength of saturated rocks compared with that of dry rocks. In the dynamic tests (Fig. 13a), the initiation and propagation of rock fractures can be delayed by the viscous behavior

of free water between the grains, including the flowing three parts: (1) σ_1 , resisting stress induced by the meniscus effect (Rossi 1991 and Wang et al. 2009), as shown in Fig. 13a, the free water fails to get to the new-formed cracks during dynamic loading, where a meniscus is formed to provide the resisting stress; (2) σ_2 , resisting stress induced by the Stefan effect (Zheng and Li 2004), which can be graphically interpreted in Fig. 13c. The free water between the two plates would provide such resisting stress, when the vertically relative motion happens on the two plates. (3) σ_3 , resisting stress induced by Newton inner friction effect (Franzini 1975), which can be graphically interpreted in Fig. 13d. the water between the two plates would produce another resisting stress, when parallelly relative motion happens on the two plates. In the repetitive impacting tests (Fig. 13b), the free water in the specimen can diffuse to the new-formed crack tips after each impact. After the external loading, the free water between the grains leads to the pore water pressure (crack splitting stress, σ_4), which further promotes the crack propagation and decreases the compressive strength

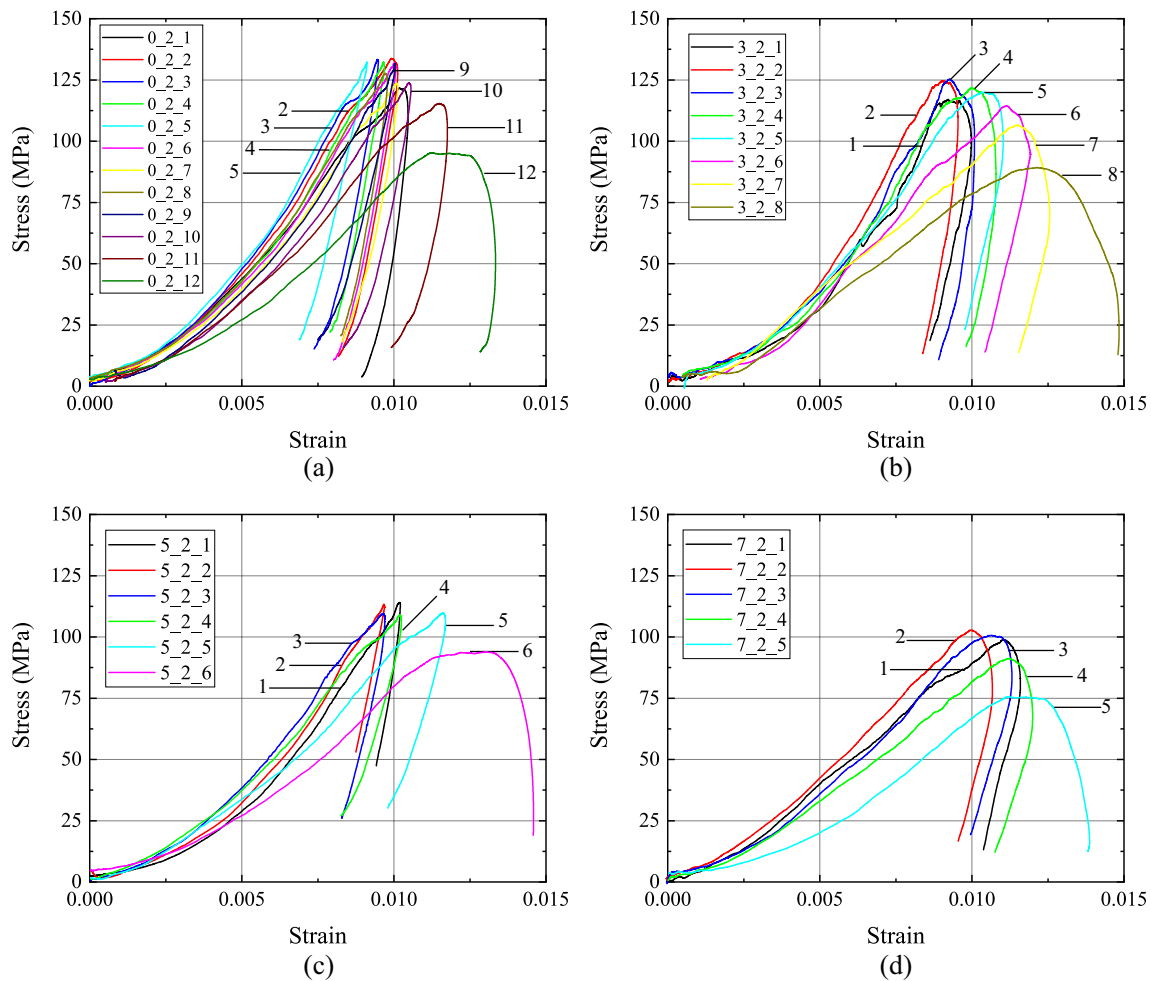


Fig. 7 Stress–strain curves of **a** 0°, **b** 3°, **c** 5° and **d** 7° specimen under the dynamic loading rate of ~950 GPa/s

of rock. Subsequently, the meniscus effect (σ_1) should be ignored considering that the free water can get to the crack tips. Comparing with the single impacting tests, the Stefan effect and Newton inner friction effect in repetitive impacting tests is much smaller due to the much lower relative velocities of the two plates in both the vertical and parallel directions.

3.3 Energy Dissipation

The dynamic energy dissipation of the saturated and dry specimen under repetitive compression–shear impacting is analyzed in this section. As shown in Fig. 14, the concerned energy evolutions at the 11th and final impacts at the loading rate of ~950 GPa/s are employed to evaluate the energy dissipation of the saturated and dry 0° specimen. Upon the arrival of the incident wave at the bar–specimen interface, the incident energy was divided into three parts: (i) the main part reflected into the incident bar forming the reflected energy; (ii) after several microseconds, the stress

wave propagated at the transmitted end of the specimen, and the part of the energy stored in the specimen was released forming the transmitted energy; and (iii) the and the rest absorbed by the specimen forming the absorbed energy. From the dynamic loading applied on the specimen, the evolution curves of reflected energy, the absorbed energy, and the transmitted energy rise up successively, and the slowing growth of the reflected energy and absorbed energy accelerated the growth of transmitted energy. It is worth noting that the absorbed energy decreases obviously after its peak value, and the slope of the curve for incident energy also decreases. This phenomenon is believed to be a significant result of the rebound effect, and the insufficient input energy in the specimen is not enough to offset the releasing elastic energy. In the final impact, the evolution of absorbed energy almost remains constant after a monotonously increased process.

The reflected, transmitted, and absorbed energies were normalized by the incident energy to analyze the energy dissipation of saturated rocks under repetitive impacting. Figures 15a, b depict the representative energy evolution

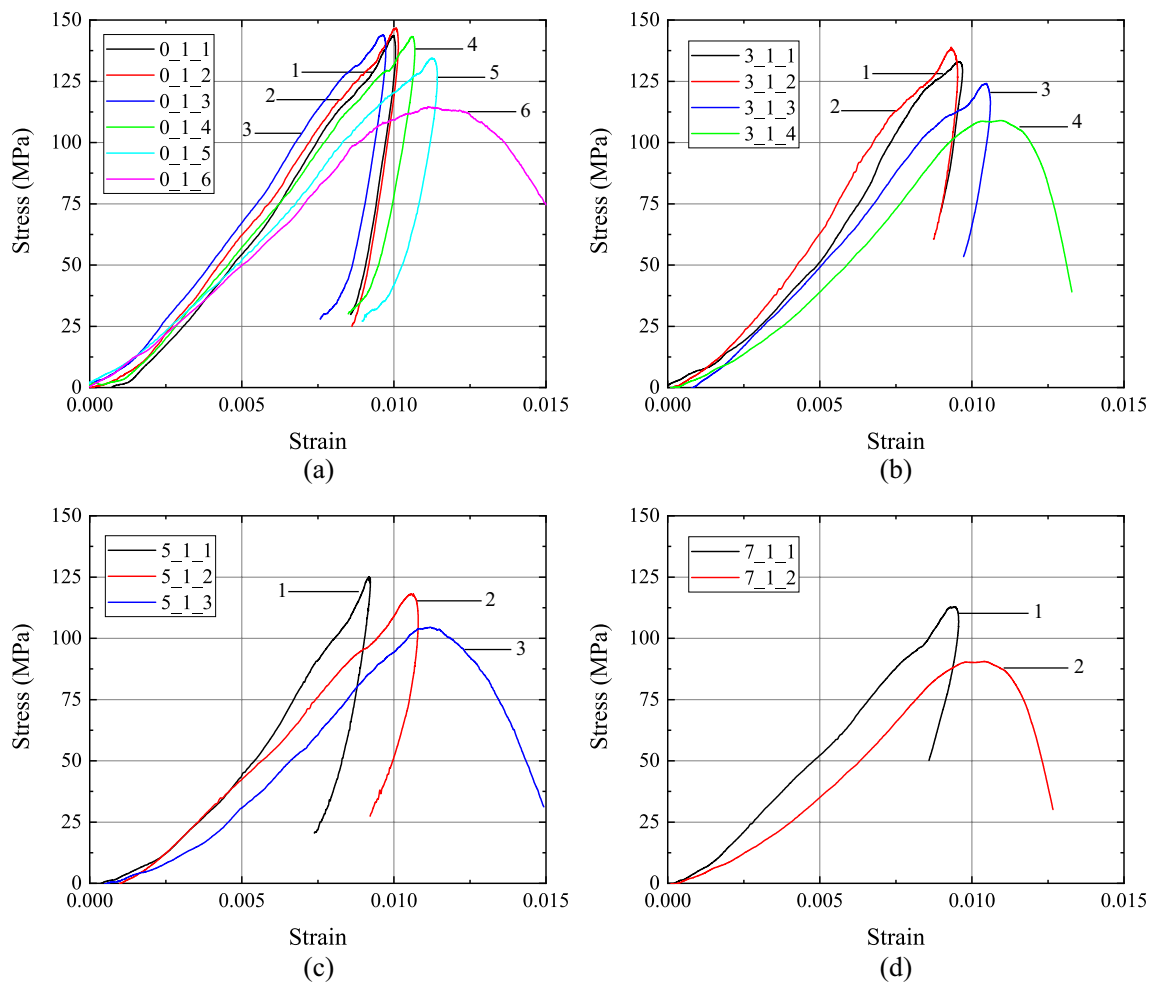


Fig. 8 Stress–strain curves of **a** 0°, **b** 3°, **c** 5° and **d** 7° specimen under the dynamic loading rate of ~ 1200 GPa/s

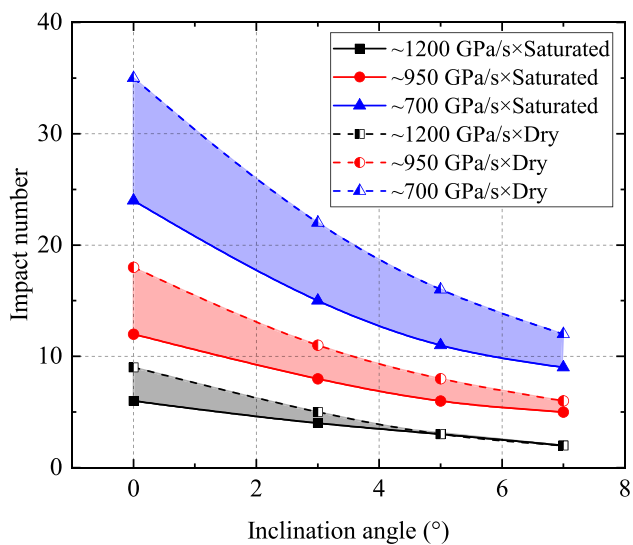
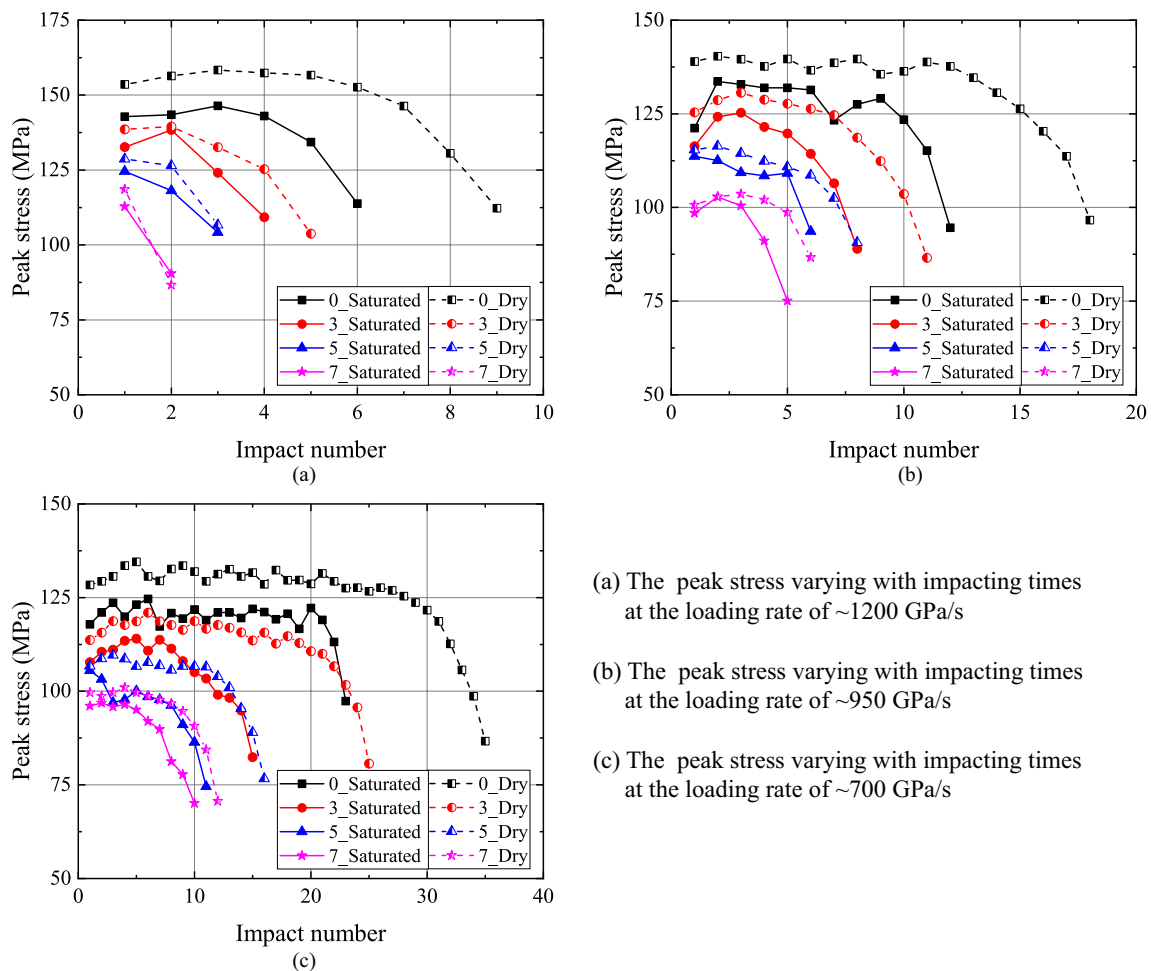


Fig. 9 Impact number of saturated and dry 0°, 3°, 5°, and 7° specimens under different loading rates

curves versus impact number of the saturated and dry 0° specimen at the loading rate of ~ 950 GPa/s. In both water content conditions, a large part of the incident energy is reflected back to the bar and transmitted through the specimen, for example, in the sixth impact, the transmitted energy and reflected energy account for 75% and 21%, respectively. A small portion of the energy (less than 10%) is absorbed by the specimen for the microscopic damage and the macrocrack propagation, especially in the middle of several impacts. The absorbed energy proportion of dry rocks is much smaller than these of saturated rocks, which indicates that the endurance capacity of dry rocks is higher than the saturated ones. The incident energy of saturated rocks under repetitive impacting mainly dissipates by the reflected energy and transmitted energy, and a minor part is absorbed by the specimen. Thus, we can imply that, in the mechanical rocks breaking of the waterway regulation projects, the incident energy from the drop hammer or impact drilling is mainly dissipated in the form of seismic waves expanding outward and reflected stress wave propagating back to the



(a) The peak stress varying with impacting times at the loading rate of ~1200 GPa/s
 (b) The peak stress varying with impacting times at the loading rate of ~950 GPa/s
 (c) The peak stress varying with impacting times at the loading rate of ~700 GPa/s

Fig. 10 Dynamic peak stress of the saturated and dry inclined specimen under repetitive impacting at the different loading rates

hammer, rather than consumed by the crack generation and propagation in the submerged reefs. Figure 15c, d demonstrates the energy density and cumulative energy density against the impact number of saturated and dry rocks. Similar to Li et al. (2018a, b), the energy density varying with the impacting numbers can be divided into three stages: (i) the energy density decreases as the impact number increases at the first several impacts, and the cumulative energy density increases slowly; (ii) the energy density fluctuates around 0.06 J/cm³ with minor amplitude, and the cumulative energy density quasi-linearly increases; and (iii) the energy density exhibits a significant increase at the final several impacts, and the cumulative energy density increases rapidly. The cumulative energy density of dry rocks is larger than that of saturated rocks, which suggests that more energy would be consumed for the rock breaking in dry condition.

To investigate the effect of shear composition in the dynamic impacting on the energy dissipation of saturated and dry inclined rock specimens, the energy utilization

varying with impact number is plotted in Fig. 16. A similar trend for the energy utilization of specimens with different tilting angles against the impact number was observed, and it decreases at the first several impacts and sharply increases at the final several impacts. As the tilting angle of the specimen increases, the energy utilization of saturated rocks under repetitive impacting exhibits a rapid increase from less than 10% for the 0° specimen to more than 20% for 7° inclined specimen. It is worth noting that the increment of energy utilization obviously decreases as the tilting angle increases, and exemplar of the 5° specimen is in accordance with that of the 7° specimen. We can imply that the energy utilization improvement of saturated rocks under repetitive impacting by increasing the shear/compressive ratio of the dynamic loading yields an ascension limit. For a higher energy utilization in the mechanical rock breaking of the waterway regulation projects, the oblique strike of the drop hammer or impact drilling should be implemented, and the 5° or 7° tilting angle might be the optimal.

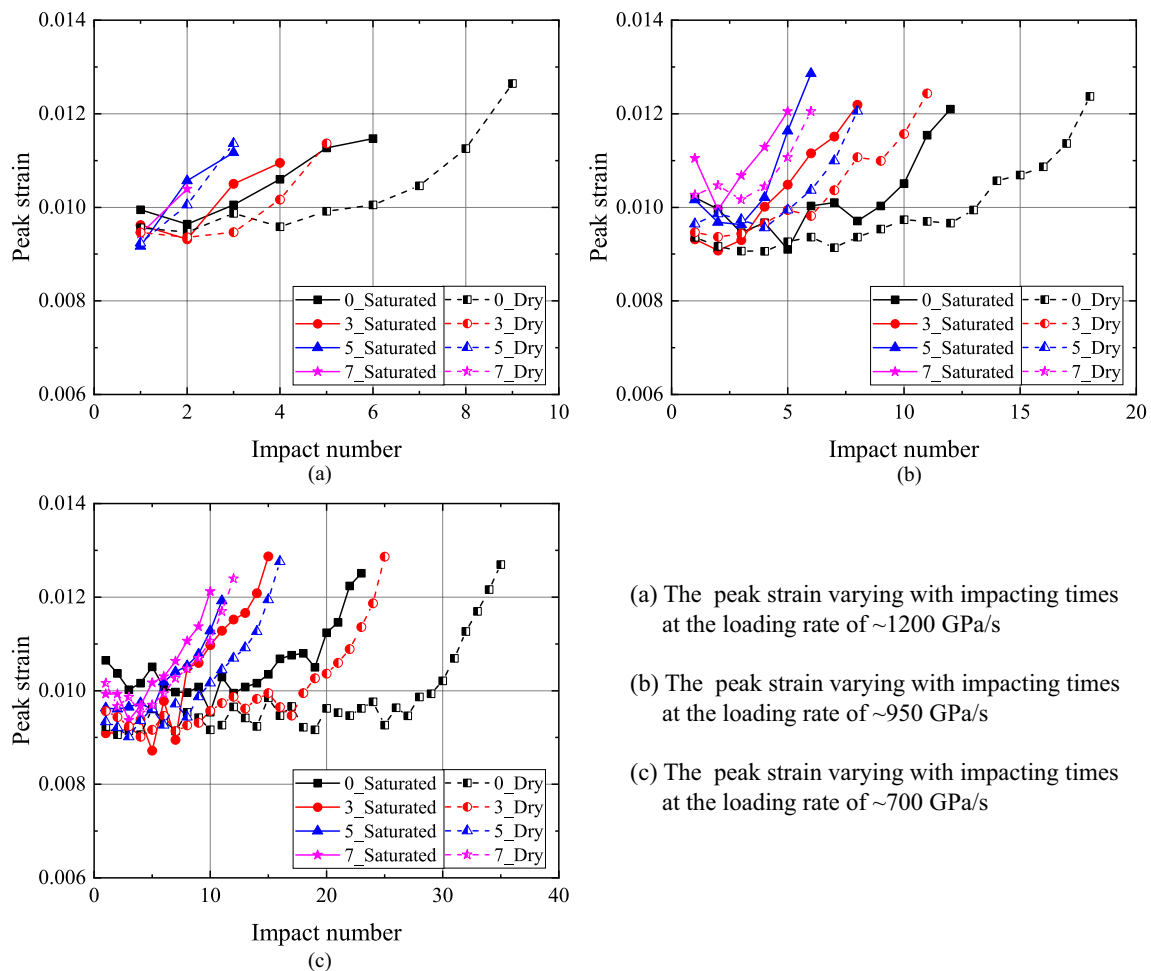


Fig. 11 Dynamic peak strain of the saturated and dry inclined specimen under repetitive impacting at the different loading rates

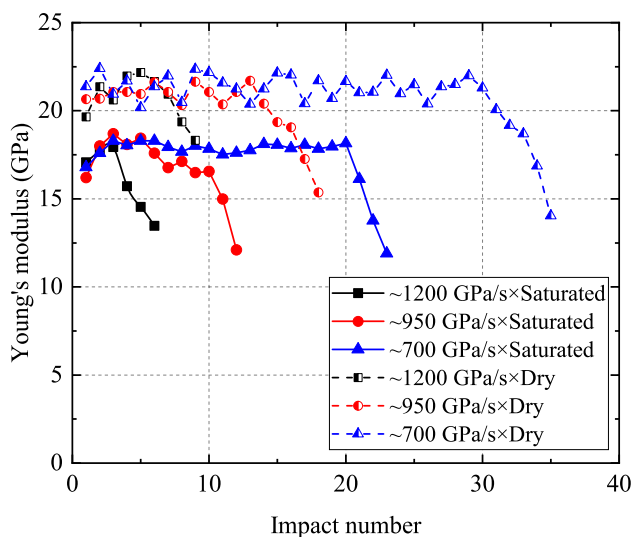


Fig. 12 Dynamic Young's modulus of saturated and dry sandstone under repetitive impacting at the different loading rates

3.4 Failure Patterns

To investigate the effect of the repetitive compression–shear impacting on the failure patterns of saturated and dry rocks, the photographs of specimens with tilting angles of 0° and 5° after several impacts were compared in Fig. 17, in which the full-field strain of the specimen surface is calculated using the open-source DIC algorithm (Zhang et al. 2022). For the cubical specimen (0°) in dry and saturated conditions, the strain was first concentrated on the transmitted end of the specimen and then propagated to the incident end, forming a large deformation band along the loading direction. According to the crack types defined by Liu et al. (2018), Yan et al. (2021) and Liu and Dai (2021), the right cuboid specimens show an evident splitting failure along the loading direction in both saturated and dry conditions. For the inclined specimen in dry condition, it is observable that the rock specimen feature the mixed failure mode of tensile and shear failure with a single shear band, and the shear failure mode becomes more dominant with increasing the tilting

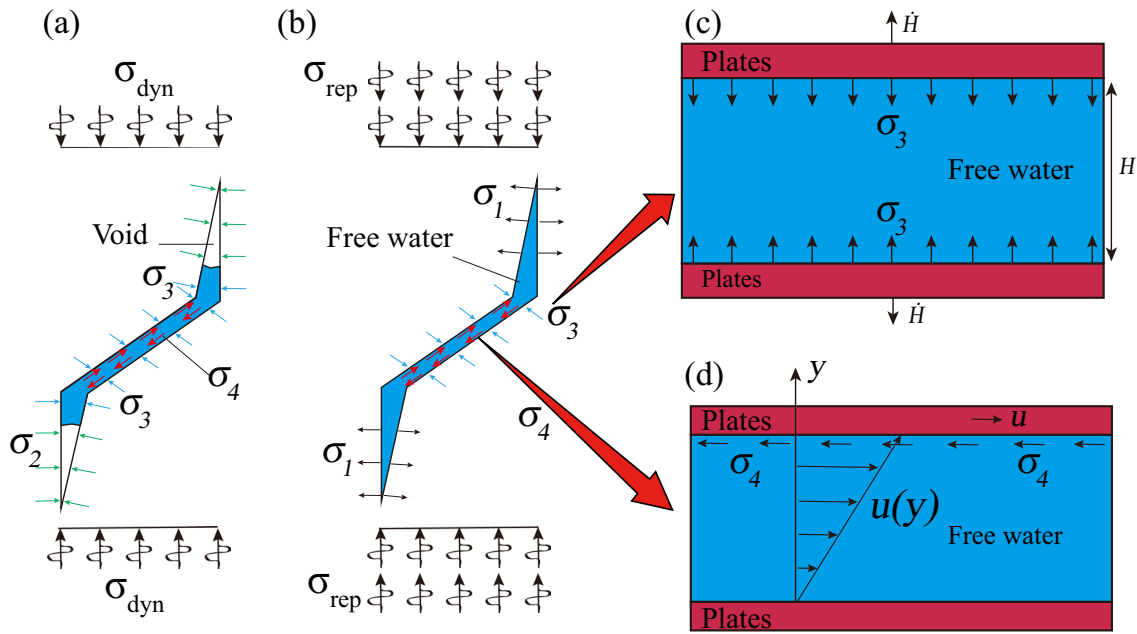


Fig. 13 a Stresses induced by water in a dynamic tests and b repetitive impacting tests, including the resisting stresses induced by c Stefan effect (σ_2) and d by Newton inner friction effect (σ_3)

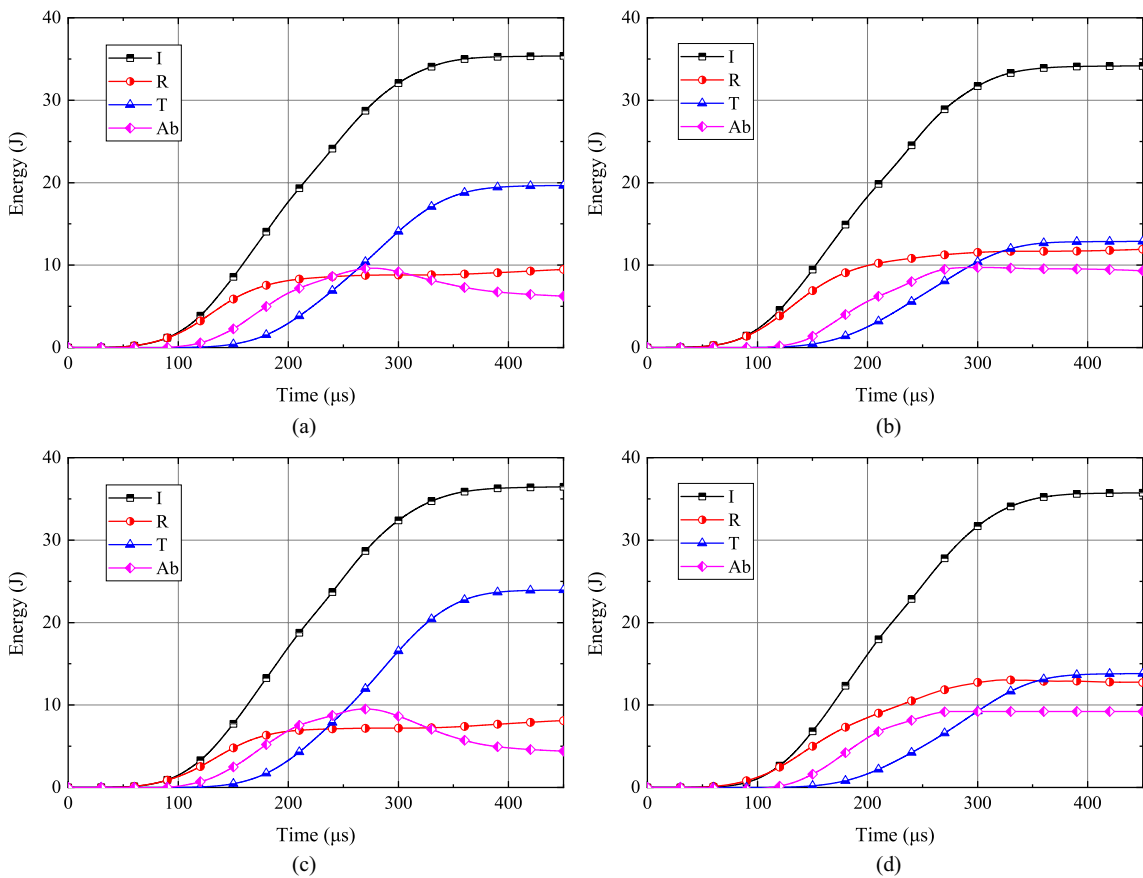


Fig. 14 Energy evolution of saturated 0° specimen at a 11th and b final impacts and of dry 0° specimen at c 11th and d final impacts at the loading rate of ~ 950 GPa/s

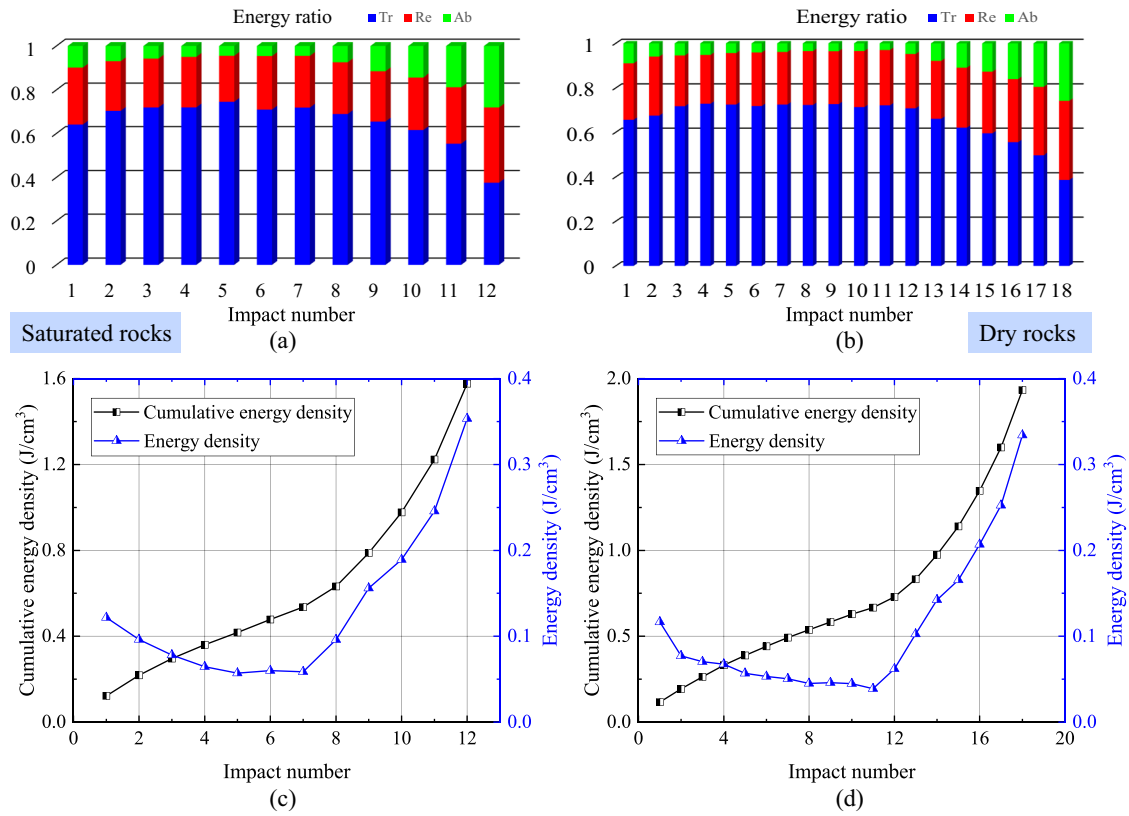


Fig. 15 Energy partition and density varying with impact number of saturated and dry 0° specimens at the loading rate of ~950 GPa/s

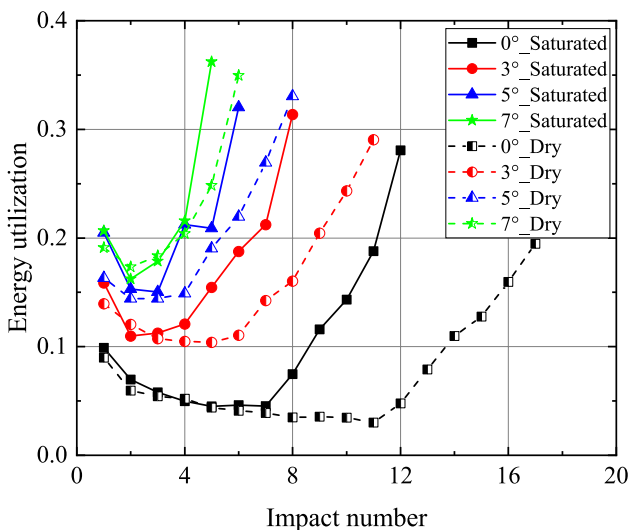


Fig. 16 Energy utilization varying with impact number of the saturated and dry inclined specimens at the loading rate of ~950 GPa/s

angle. For the inclined specimen in saturated condition, the strain was first concentrated on the two obtuse corners of the specimen and then propagated to another end of the specimen, forming two parallel large deformation bands with a

large tilting angle to the loading direction. Thus, the failure patterns of rocks change from the relative tensile mode to the combined compression–shear mode as the shear component is introduced into the impact loading, and the water content between the mineral grains promotes the shear failure in rock dynamic testing. Besides, this might be the deep reason for the improvement of the energy utilization and the weakness of the bearing capacity as the shear/compressive ratio increases.

For a better understanding of the failure mechanism of dry and saturated rocks under static and dynamic loading conditions, the optical microscopic morphologies from scanning electron microscope (SEM) have been shown in Fig. 18, in which TG and IG represent the trans-granular and inter-granular fractures, respectively. More IG fractures could be observed on the fracture surface as the rocks change from dry into saturated condition in both the static and dynamic tests, and this indicates that the TG fracturing is suppressed in saturated samples but the IG dilation is the dominant deformation mechanism. As the loading changed from static into dynamic condition, more TG fractures on the fracture surface can be observed. It suggests that the TG fracturing is promoted by the dynamic loading, and the TG as well as IG crack shares the responsibility for

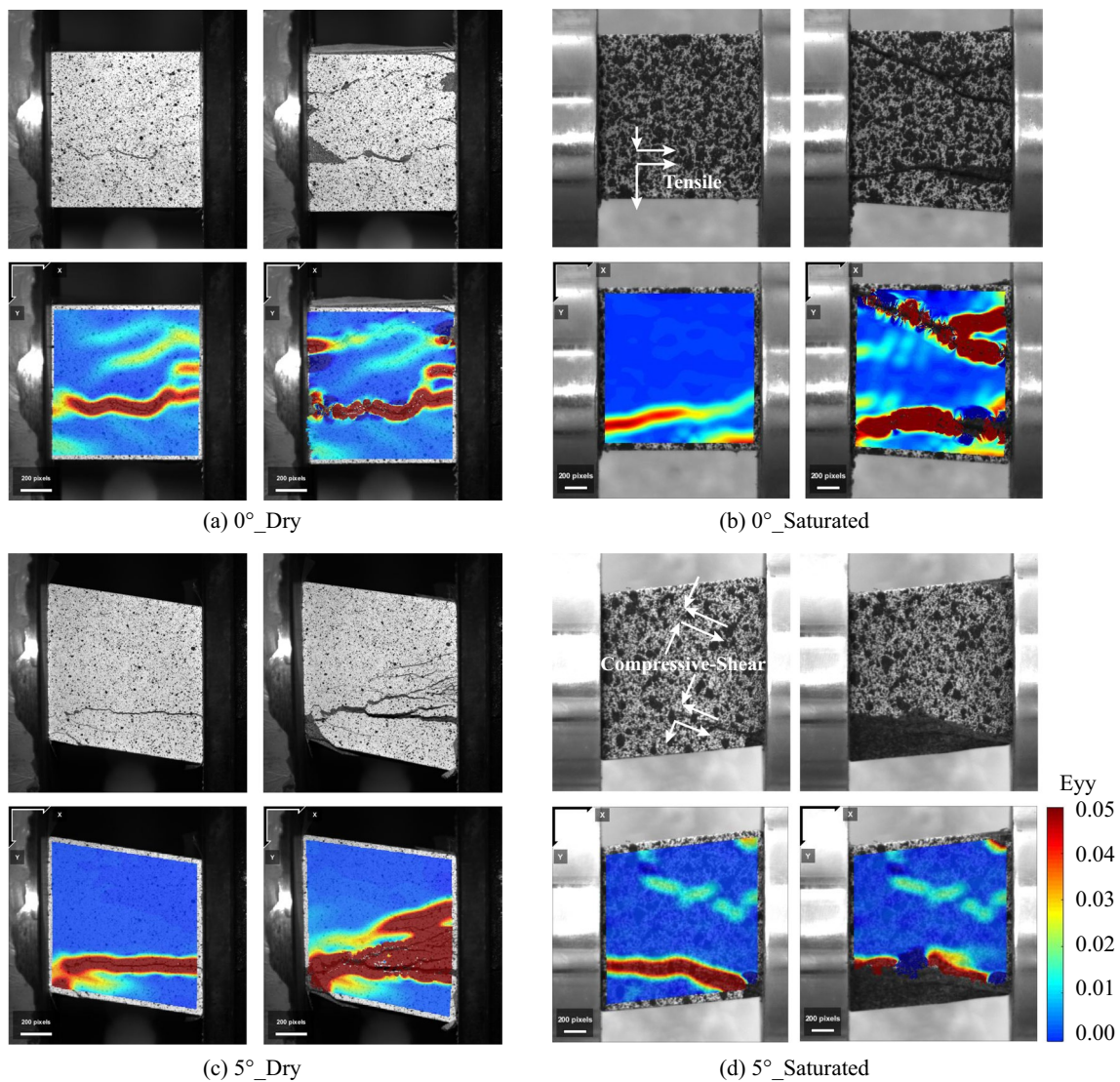


Fig. 17 The photographs and the full-field strain of 0° and 5° specimens in dry and saturated conditions

the rock fracturing. The sandstone is composed of mineral grains and cement between grains, the schematic diagrams of IG/TG fractures have been proposed to further explain this phenomenon. As shown in Fig. 13a, b, the water content between the grains can increase the internal porosity of sandstone due to the physical and chemical reactions, resulting the increasingly loose of rock structures and the gradually weakening of grains cementation (Li et al. 2018a, b; Cai et al. 2020; Liu et al. 2022). Thus, the cracks more likely propagate along the cementation, forming more IG fractures. As shown in Fig. 13b, c, internal stress of sandstone increases as the loading state changed from static into high loading rate impacting, resulting in increasing interaction between grains. Thus, when such interaction exceeds the bearing capacity of grains, the grains would break and the cracks could propagate through grains, forming the TG

fractures (Fig. 19). Therefore, under higher loading rates or saturated condition, more TG fractures occur on the fracture surface of the failed specimen.

4 Conclusions

Submerged reefs are likely subjected to the repetitive oblique impacting from the drop hammer or the impact drilling in the rock breaking of the waterway regulation projects. To investigate the dynamic responses and failure behaviors of saturated rocks under repetitive combined compression–shear loading, the repetitive impacting tests were thus carried out on specimens with different tilting angles using the SHPB apparatus. The dynamic stress equilibrium

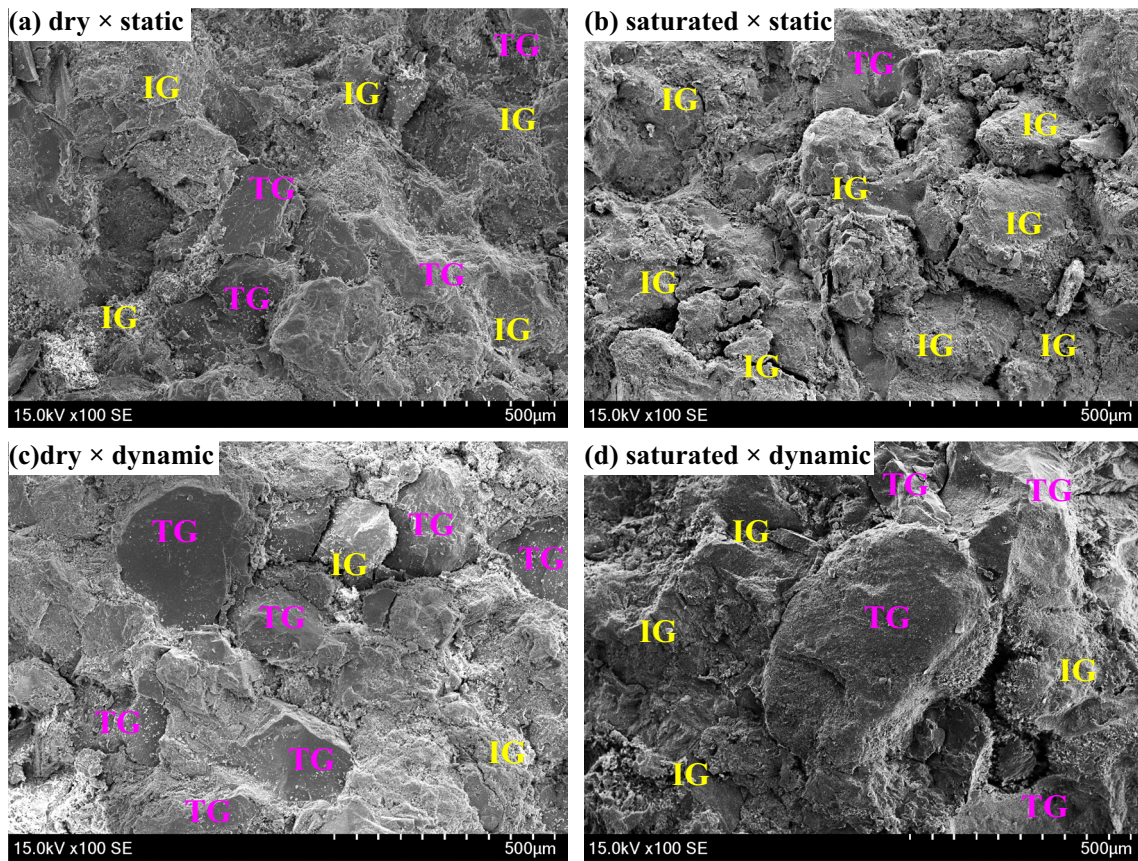


Fig. 18 Microscopic morphologies of **a** dry and **b** saturated rocks under static loading condition, and **c** dry and **d** saturated rocks under dynamic loading condition (TG and IG represent trans-granular fracture and inter-granular fracture, respectively)

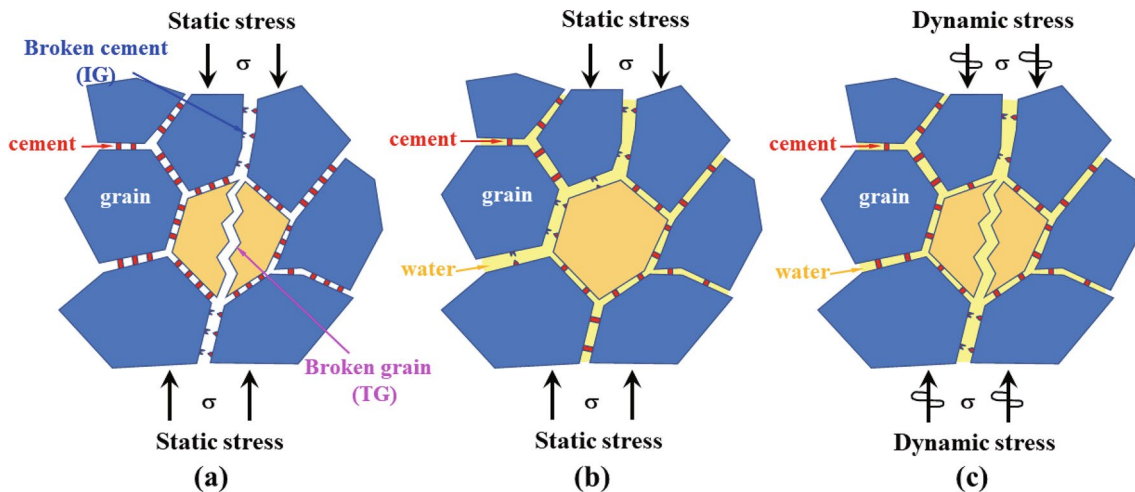


Fig. 19 The schematic diagram of IG/TG fracture of sandstone in different loading conditions

of inclined saturated rock specimen subjected to repetitive compression–shear impacting can be effectively satisfied by virtue of the pulse shaping technique.

Experimental results show that the introduction of the shear component in the repetitive impacting has significant

influences on the loading bearing capacity, the deformation property, the energy dissipation law, and the failure patterns of saturated rocks under repetitive impacting. As the repetitive impacting acts on the saturated sandstone, its bearing capacity decreases, while the deformability increases. The

increasing shear component and loading rate has a negative influence on the endurance of saturated sandstone under repetitive impacting. The incident energy of saturated sandstone under repetitive impacting mainly dissipates by the reflected energy and transmitted energy rather than the absorbed energy. The increasing shear component in the dynamic loading improves the energy absorption ability and the energy utilization of the saturated sandstone. The failure patterns of saturated rocks change from the relative tensile mode with a large deformation band along the loading direction to the combined compression–shear mode with two parallel large deformation bands inclined to the loading direction as the shear component introduces into the dynamic loading, and the water content between the mineral grains promotes the shear failure in rock dynamic testing.

Acknowledgements The authors thank the financial support from the National Outstanding Youth Science Fund Project of National Natural Science Foundation of China (52225904), the Natural Science Foundation of China (52209121), Natural Science Foundation of Chongqing (cstc2021jcyj-msxmX0952), the Youth Science and Technology Innovation Research Team Fund of Sichuan Province (2020JDTD0001).

Data Availability Statement Data and material used in preparation of this manuscript are available from the corresponding authors upon reasonable request if not already in the public domain.

Declarations

Conflict of interest All authors declare that they have no known competing financial interests or personal relationships that could have appeared to influence the work reported in this paper.

References

- Ali AB, Mohammed H (2021) A review of some nonexplosive alternative methods to conventional rock blasting. *Open Geosci* 13:431–442
- Baud P, Zhu WL, Wong TF (2000) Failure mode and weakening effect of water on sandstone. *J Geophys Res* 105:16371–16389
- Bomba MS, Harrison R (2002) Feasibility of a container-on-barge network along the Texas Gulf Coast. *Mar Transport Port Oper Mar Transport* 1782:23–30
- Broch E (1979) Change in rock strength by water. In: *Proceedings of 4th international society of rock mechanics, Montreux*, pp 71–75
- Bu F, Nachtmann H (2021) Literature review and comparative analysis of inland waterways transport: “Container on Barge.” *Marit Econ Logist*. <https://doi.org/10.1057/s41278-021-00195-6>
- Cai X, Zhou Z, Du X, Zang H (2019) Water-weakening effects on the mechanical behavior of different rock types: phenomena and mechanisms. *Appl Sci* 9:4450
- Cai X, Zhou ZL, Zang HZ, Song ZY (2020) Water saturation effects on dynamic behavior and microstructure damage of sandstone: phenomena and mechanisms. *Eng Geol* 276:105760
- Dai F, Zhang Q, Liu Y, Du HB, Yan ZL (2022) Experimental evaluation of sandstone under cyclic coupled compression–shear loading: fatigue mechanical response and failure behavior. *Acta Geotech* 17:3315–3336
- Du HB, Dai F, Xu Y, Liu Y, Xu HN (2018) Numerical investigation on the dynamic strength and failure behavior of rocks under hydrostatic confinement in SHPB testing. *Int J Rock Mech Min* 108:43–57
- Du HB, Dai F, Xu Y, Yan ZL, Wei MD (2020) Mechanical responses and failure mechanism of hydrostatically pressurized rocks under combined compression–shear impacting. *Int J Mech Sci* 165:105219
- Du HB, Dai F, Wei MD, Li A, Yan ZL (2021) Dynamic compression–shear response and failure criterion of rocks with hydrostatic confining pressure: An experimental investigation. *Rock Mech Rock Eng* 54:955–971
- Erguler ZA, Ulusay R (2009) Water-induced variations in mechanical properties of clay-bearing rocks. *Int J Rock Mech Min Sci* 46:355–370
- Fazi S, Fransoo JC, Woensel TV (2015) A decision support system tool for the transportation by barge of import containers: a case study. *Decis Support Syst* 79:33–45
- Feng P, Zhao J, Dai F, Wei MD, Liu B (2021) Mechanical behaviors of conjugate-flawed rocks subjected to coupled static–dynamic compression. *Acta Geotech* 17:1765–1784
- Franzini JB (1975) *Fluid mechanics with engineering applications*. Tata McGraw-Hill Education, New York
- Frew DJ, Forrestal MJ, Chen W (2002) Pulse shaping techniques for testing brittle materials with a split Hopkinson pressure bar. *Exp Mech* 42(1):93–106
- Gharehgozli A, Zaerpour N (2018) Stacking outbound barge containers in an automated deep-sea terminal. *Eur J Oper Res* 267(3):977–995
- Hawkins AB, McConnell BJ (1992) Sensitivity of sandstone strength and deformability to changes in moisture content. *Q J Eng Geol* 25(2):115–130
- Hong L, Zhou ZL, Yin TB, Liao GY, Ye ZY (2009) Energy consumption in rock fragmentation at intermediate strain rate. *J Cent South Univ Technol* 16:0677–0682
- Hou B, Ono A, Abdennadher S, Pattofatto S, Li YL, Zhao H (2011) Impact behavior of honeycombs under combined shear–compression. Part I: experiments. *Int J Solids Struct* 48(5):687–697
- Hou B, Xiao R, Sun TF (2019) A new testing method for the dynamic response of soft cellular materials under combined shear–compression. *Int J Mech Sci* 159:306–314
- Johnson PA, Jia X (2005) Nonlinear dynamics, granular media and dynamic earthquake triggering. *Nature* 437:871–874
- Kawai K, Sakuma H, Katayama I, Tamura K (2015) Frictional characteristics of single and polycrystalline muscovite and influence of fluid chemistry. *J Geophys Res Solid Earth* 120:6209–6218
- Kolsky H (1949) An investigation of the mechanical properties of materials at very high rates of loading. *Proc Phys Soc Sect B* 62(11):676–700
- Li XB, Lok TS, Zhao J (2005) Dynamic characteristics of granite subjected to intermediate loading rate. *Rock Mech Rock Eng* 38(1):21–39
- Li D, Wong LNY, Liu G, Zhang X (2012) Influence of water content and anisotropy on the strength and deformability of low porosity meta-sedimentary rocks under triaxial compression. *Eng Geol* 126:46–66
- Li XF, Li X, Li HB, Zhang QB, Zhao J (2018a) Dynamic tensile behaviours of heterogeneous rocks: the grain scale fracturing characteristics on strength and fragmentation. *Int J Impact Eng* 118:98–118
- Li SH, Zhu WC, Niu LL, Yu M, Chen CF (2018b) Dynamic characteristics of green sandstone subjected to repetitive impact loading: phenomena and mechanisms. *Rock Mech Rock Eng* 51:1921–1936

- Li JC, Rong LF, Li HB, Hong SN (2019) An SHPB test study on stress wave energy attenuation in jointed rock masses. *Rock Mech Rock Eng* 52:403–420
- Liu Y, Dai F (2021) A review of experimental and theoretical research on the deformation and failure behavior of rocks under cyclic loads. *J Rock Mech Geotech Eng* 13(5):1203–1230
- Liu Y, Dai F, Dong L, Xu NW, Feng P (2018) Experimental investigation on the fatigue mechanical properties of intermittently jointed rock models under cyclic uniaxial compression with different loading parameters. *Rock Mech Rock Eng* 51:47–68
- Liu XY, Liu Y, Dai F, Yan ZL (2022) Tensile mechanical behavior and fracture characteristics of sandstone exposed to freeze-thaw treatment and dynamic loading. *Int J Mech Sci* 226:107405
- Luo XD, Jiang N, Wang MY, Xu Y (2016) Response of leptynite subjected to repeated impact loading. *Rock Mech Rock Eng* 49:4137–4141
- Rossi P (1991) A physical phenomenon which can explain the mechanical behaviour of concrete under high strain rates. *Mater Struct* 24(24):422–424
- Talesnick M, Shehadeh S (2007) The effect of water content on the mechanical response of a high-porosity chalk. *Int J Rock Mech Min Sci* 44:584–600
- Tong LH, Yu Y, Lai SK, Lim CW (2019) Dynamic weakening of sandstone subjected to repetitive impact loading. *Rock Mech Rock Eng* 52:2197–2206
- Vásárhelyi B (2005) Statistical analysis of the influence of water content on the strength of the Miocene limestone. *Rock Mech Rock Eng* 38(1):69–76
- Vásárhelyi B, Ván P (2006) Influence of water content on the strength of rock. *Eng Geol* 84:70–74
- Wang H, Jin W, Li Q, Li QB (2009) Saturation effect on dynamic tensile and compressive strength of concrete. *Adv Struct Eng* 12(2):279–286
- Wang Y, Zhou X, Kou M (2019) Three-dimensional numerical study on the failure characteristics of intermittent fissures under compressive-shear loads. *Acta Geotech* 14(4):1161–1193
- Wang SM, Xiong XR, Liu YS, Zhou J, Du K, Cui Y, Khandelwal M (2021) Stress-strain relationship of sandstone under confining pressure with repetitive impact. *Geomech Geophys Geo Energy Geo Resour* 7:39
- Wasantha PLP, Ranjith PG, Permata G, Bing D (2018) Damage evolution and deformation behaviour of dry and saturated sandstones: insights gleaned from optical measurements. *Meas J Int Meas Confed* 130:8–17
- Wong LNY, Maruvanchery V, Liu G (2016) Water effects on rock strength and stiffness degradation. *Acta Geotech* 11:713–737
- Wu BB, Kanopoulos P, Luo XD, Xia KW (2014) An experimental method to quantify the impact fatigue behavior of rocks. *Meas Sci Technol* 25:075002
- Xiao Y, Yuan Z, Chu J (2019) Particle breakage and energy dissipation of carbonate sands under quasi-static and dynamic compression. *Acta Geotech* 14:1741–1755
- Xu Y, Dai F (2018) Dynamic response and failure mechanism of brittle rocks under combined compression-shear loading experiments. *Rock Mech Rock Eng* 51(3):747–764
- Xu S, Huang J, Wang P, Zhang C, Zhou L, Hu S (2015) Investigation of rock material under combined compression and shear dynamic loading: an experimental technique. *Int J Impact Eng* 86:206–222
- Xu Y, Dai F, Du HB (2020) Experimental and numerical studies on compression-shear behaviors of brittle rocks subjected to combined static-dynamic loading. *Int J Mech Sci* 175:105520
- Xu Y, Pellegrino A, Dai F, Du HB (2021) Experimental and numerical investigation on the dynamic failure envelope and cracking mechanism of pre-compressed rock under compression-shear loads. *Int J Geomech* 21(11):04021208
- Yan ZL, Dai F, Liu Y, Du HB (2020) Experimental investigations of the dynamic mechanical properties and fracturing behavior of cracked rocks under dynamic loading. *Bull Eng Geol Environ* 79:5535–5552
- Yan ZL, Dai F, Liu Y, Li YZ, You W (2021) Experimental investigation of pre-flawed rocks under combined static-dynamic loading: mechanical responses and fracturing characteristics. *Int J Mech Sci* 211:160755
- Yilmaz I (2010) Influence of water content on the strength and deformability of gypsum. *Int J Rock Mech Min Sci* 47:342–347
- You W, Dai F, Liu Y, Yan Z (2022) Effect of confining pressure and strain rate on mechanical behaviors and failure characteristics of sandstone containing a pre-existing flaw. *Rock Mech Rock Eng* 55(4):2091–2109
- Zhang Q, Dai F, Liu Y (2022) Experimental assessment on the dynamic mechanical response of rocks under cyclic coupled compression-shear loading. *Int J Mech Sci* 216(15):106970
- Zhao PD, Lu FY, Chen R (2011) A technique for combined dynamic compression-shear test. *Rev Sci Instrum* 82(3):35110
- Zhao PD, Lu FY, Lin YL, Chen R, Li JL, Lu L (2012) Technique for combined dynamic compression-shear testing of PBXs. *Exp Mech* 52(2):205–213
- Zhou YX, Xia KW, Li XB, Li HB, Ma GW, Zhao J, Zhou ZL, Dai F (2012) Suggested methods for determining the dynamic strength parameters and mode-I fracture toughness of rock materials. *Int J Rock Mech Min* 49:105–112
- Zhou ZL, Cai X, Zhao Y, Chen L, Xiong C, Li XB (2016a) Strength characteristics of dry and saturated rock at different strain rates. *Trans Nonferrous Metal Soc* 26:1919–1925
- Zhou ZL, Cai X, Cao WZ, Li XB, Xiong C (2016b) Influence of water content on mechanical properties of rock in both saturation and drying processes. *Rock Mech Rock Eng* 49(8):3009–3025
- Zhou ZL, Cai X, Chen L, Cao WZ, Zhao Y, Xiong C (2017) Influence of cyclic wetting and drying on physical and dynamic compressive properties of sandstone. *Eng Geol* 220:1–12
- Zweers BG, Bhulai S, Vander Mei RD (2019) Optimizing barge utilization in hinterland container transportation. *Nav Res Logist* 66(3):253–271

Publisher's Note Springer Nature remains neutral with regard to jurisdictional claims in published maps and institutional affiliations.

Springer Nature or its licensor (e.g. a society or other partner) holds exclusive rights to this article under a publishing agreement with the author(s) or other rightsholder(s); author self-archiving of the accepted manuscript version of this article is solely governed by the terms of such publishing agreement and applicable law.